Melt Pool Acquisition Using Near-Infrared Camera in Aluminum Wire Arc Additive Manufacturing

Anthony Dellarre[(✉)], Maxime Limousin, and Nicolas Beraud

(Institute of Engineering Univ. Grenoble Alpes), Univ. Grenoble Alpes, Grenoble INP, 38000 Grenoble, France
anthony.dellarre@grenoble-inp.fr

Abstract. In order to produce functional parts in Wire Arc Additive Manufacturing (WAAM), mastering parts quality is a key challenge. The literature highlights the connection between thermal conditions and part defects. Thus, monitoring a thermal parameter, for instance the melt pool in this study, is a crucial indicator to describe parts quality. The paper aims to investigate the feasibility of CMOS camera (Complementary Metal–Oxide–Semiconductor) to track a homothety of the melt pool for parts manufactured by WAAM. In this field, the literature still lacks information concerning this sensor operating in industrial condition, especially for aluminum alloys. An experiment and a numerical method are developed to estimate its sensitivity and robustness. Validation criteria for the method are presented and confirm its interest.

Keywords: WAAM · Monitoring · Near infrared camera · Thermal · Aluminum

1 Introduction

WAAM (Wire Arc Addictive Manufacturing) is an established additive manufacturing process. It can produce complex and large parts by superposing metal bead layer by layer. Material and energy are provided by the torch mounted on a robot or Computer Numerical Control machine (CNC). Several solutions are available for the modulation of the input energy [1]. Cold Metal Transfer (CMT) is one of these solutions. It has low heat input, no splatter and high process tolerance compared to other energy sources. Its particularity is to link the displacement of the wire with an electric cycle as illustrated in Fig. 1. Several materials are available with this solution such as steel or aluminum alloys.

Nevertheless, multiple defects are not mastered during manufacturing such as porosity [3, 4], residual stresses and distortions [5] or dimensional defects [6]. Their origin is mainly due to poor thermal management during the deposition. Manokruang illustrates this relation in regard to dimensional defects by measuring the bead dimensions as a function of the substrate temperature [7].
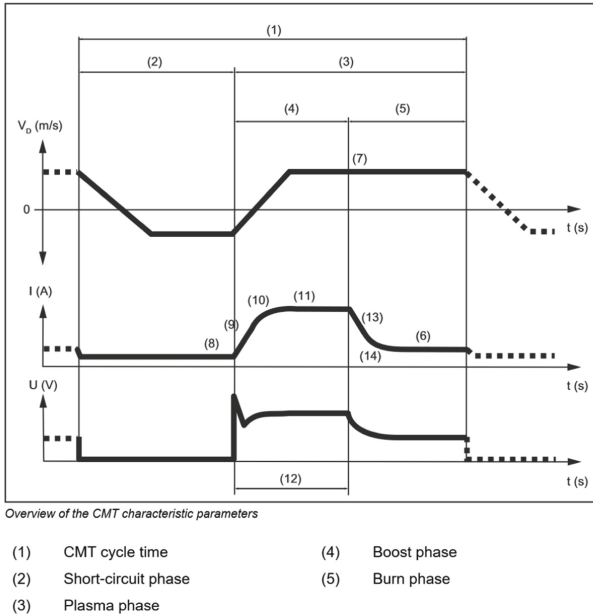
Overview of the CMT characteristic parameters

(1)	CMT cycle time	(4)	Boost phase
(2)	Short-circuit phase	(5)	Burn phase
(3)	Plasma phase		

Fig. 1. CMT electric and mechanical cycles [2].

An in-process measurement can be a solution to understand and master these defects [8]. It is interesting to monitor the physical values of the melt during welding [9]. Different solutions have been developed to track them. An ultrafast camera with a laser lighting and a light filter measuring the reflection of the light on the melt pool can be used. By choosing the laser wavelength wisely, this solution is able to work independently of the electrical arc [10]. The same devices can be used with a background light source [11]. Contours of the wire and the melt pool can thus be observed depending on a specific disposition of the devices. Also, a microbolometer can be used to get the thermal field of the melt pool [12]. In another hand, the device is wide and cannot be used to manufacture in industrial conditions. Another solution is to use a regular CCD (Charge-Coupled Device) or a CMOS (Complementary Metal–Oxide–Semiconductor) camera and to measure visible and near-infrared light radiation [13]. Only global phenomena are measured around the melt pool but the device is easy to implement and is adapted to industrial conditions. Dimensional measure of the melt pool, such as length and width, can be made such as the length or the width. Literature reports this application for steel alloys [14] but not for aluminum alloys. Moreover, for both precision and robustness of the device need to be characterized.

A majority of the previous devices allows fine understanding of the melt pool in terms of scale, time or temperature. These experimental set-ups are important, depend on laboratory conditions and generate large amount of data. The aim of this study is to develop a method to measure the melt pool in order to monitor or to closed-loop control the manufacturing process for aluminum parts. Thus, the required information is a global evolution of the melt pool size. Low frequency acquisitions and general characterizations

of the melt pool are enough and a CMOS camera meets these expectations. If this solution has been approved for steel applications [13, 14], the literature still lacks information concerning aluminum melt pool tracking.

To evaluate the feasibility of CMOS cameras to monitor melt pool for aluminum alloy, the result provided by this solution must be comparable between different experiments, robust with regard to noise during welding, and sensitive to melt pool variations.

2   Experimental Set-Up

It is difficult to observe the melt pool during welding because of the electric arcs which saturate the CMOS sensor. To overcome this issue, we take advantage of a CMT characteristic, the torch creates an intermittent arc which, for aluminum alloy, starts every 20 ms and last approximately 10 ms (Fig. 1). The CMOS camera BAUMER VCXU-04M was selected with a spectral range between 400 nm and 1000 nm. It corresponds to the visible and the near-infrared spectra. Regarding the spectral emission of the melt pool, most are near infrared origins. Thanks to the Planck's law and the spectral sensitivity of the camera, the light intensity can be evaluated as a function of the temperature (Fig. 2). Indeed, the emissivity is assumed equal to 1 and great estimations are made [9]. Nevertheless, this light intensity is related to the temperature and can represent the thermal environment of the melt pool. No complementary light source is needed.

The device is placed at a fixed distance from the melt pool and shots at a constant frame rate. There is no physical trigger connected to the camera. Thus, the raw data need to be numerically sorted in order to discard low quality shots. Its process is illustrated in Fig. 3. It works in two steps. First, the mean intensity of an image is calculated. The image is removed if its mean value is under half of the maximal pixel value. This process removes most saturated pictures. However, this method does not remove the images containing the start nor the break of the electric arc. Thus, another step is needed. An area is chosen by the user and the mean intensity is measured outside it. All the mean intensities from all images are compiled in a histogram. Their distribution is then characterized by two Gaussian (Fig. 3). The first one corresponds to valid pictures and
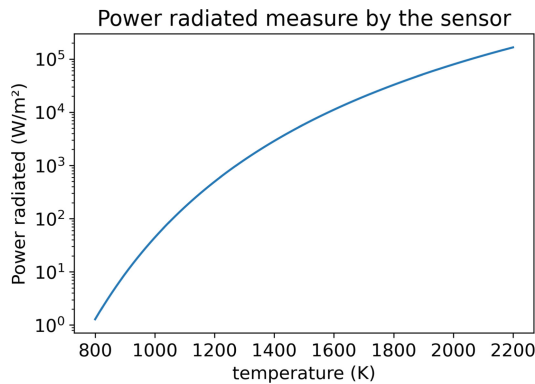

Fig. 2. Light power measure by the device

the other one to the presence of an arc or a parasite light. A threshold is set at the intersection of these two Gaussians.
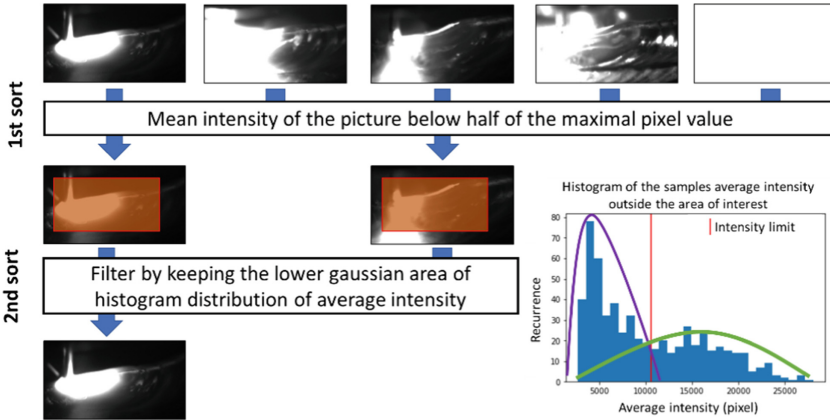

Fig. 3. Numerical sort

Then, the images are processed in order to characterize thermal areas and to compare them. As previously explained and highlighted in Fig. 2, a theoretical relation between temperature and lighting power is possible. An exponential interpolation seems relevant between 800 K to 1200 K which correspond to the aluminum liquid sate in the melt pool. So, a logarithmic treatment is applied to the image to improve the contrast. Then, a thresholding is applied. Every pixel with an intensity below 75% of the maximal value is set at 0 (Fig. 4, image processing, red line) and those above 75% are linearly distributed between 0 and the maximum (Fig. 4, image processing, green line). Finally, a threshold is applied at 15% of the maximal value (Fig. 4, threshold, red line) to select a thermal area which is compared to others during the welding process. Those thresholding values have been found experimentally as satisfying to dimensional measurement. Three dimensions are manually measured with ImageJ [15]: surface, length and height. These measures are used to describe the size of the thermal area.

To test the camera without developing a mechanical solution to fix it on the torch, the camera is installed on a tripod. Parts are produced with a 6-axis robots Yaskawa MA1440 and a left hand with 2 axes. The welding station is a Fronius T.P.S. CMT 4000 Advanced. In order to maximize the presence of the melt pool in the focal plane of the camera, a cylinder is manufactured using the left-hand plate rotation and the robot only realizes the vertical displacement. This experiment is illustrated in Fig. 5 and process parameters are detailed in Table 1. The camera parameters are in Table 2.
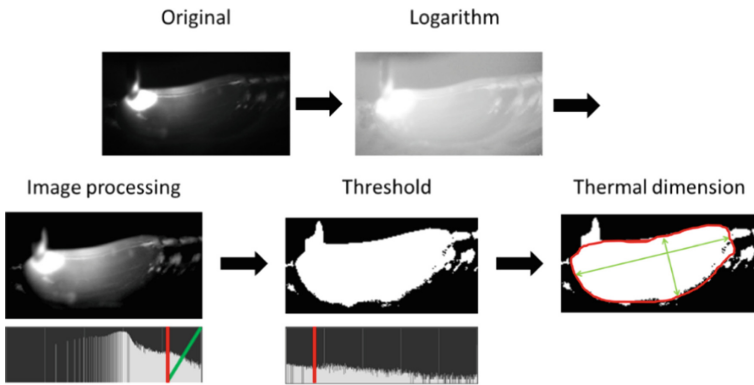
Fig. 4. Image process for valid images

Table 1. Manufacturing parameters

Weld law	Travel speed	Wire fire speed	Gas	Material	Cylinder radius
CMTP + Adv 1314	60 cm/min	6 m/min	100% Argon	AlSi4	3 cm

Table 2. Camera parameters

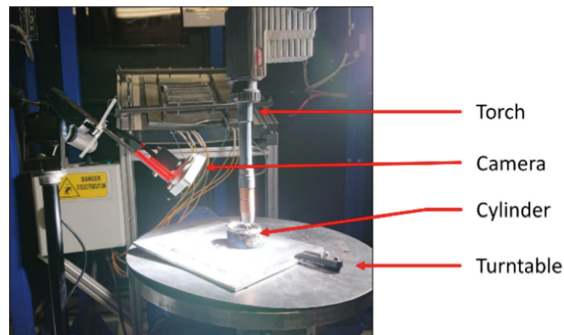| Optic	Exposition time	FPS (frame per second)	Resolution	Binning	Bit depth
F:2.0 Focal Plane: 12 mm	1.5 ms	591	208*114	Vert: 2 Horiz: 2	12 bits

Fig. 5. Camera orientation during the experiment

3   Results and Discussion

Three results are expected: a repeatable solution to compare results between them, robustness to cope with perturbations and sensibility of the melt pool size variations. Boxplots are used to format data [16].

3.1   Repeatability of the Method

To quantify the repeatability, the melt pool is filmed, and 6 valid pictures are selected. Measurements are realized 6 times for each picture using *ImageJ* [15].

For each image, the mean of all dimensions and their dispersion, equal to 2 times the standard deviation, are calculated. Then, results are merged and are presented in Table 3. A global dimension and a global dispersion are obtained. The dispersion is low enough to characterize the experience as repeatable. A comparison between the results of different experiments is possible.

Table 3. Dimensional values

Measure	Surface	Length	Height
Mean	7021	145	56
Dispersion	4%	5%	8%

3.2   Robustness of the Method

To evaluate the robustness, different kinds of simulated process noises are added to the original images. Then, processing and dimensional measurement are made following the protocol described in Sect. 2. Each measure on a noised picture is compared to the mean dimension of the reference obtained in the previous section. The deviation to the mean value for this picture is calculated and compared to the deviations presented in Table 3. According to this comparison, the method is qualified robust or not. Three kinds of noises are examined: projections during welding, size variations of the Region Of Interest (ROI) or blurry pictures.

Projection
Even if CMT welding creates few projections, some are recorded. They are small and very hot particles which saturate a small area in the picture (Fig. 6) and are still present after the numerical sort. Their influence on the outcome must be quantified. To do so, numerical artifacts are put on the same 6 images of reference. Figure 7 highlights the transformation and the experiment results are illustrated in Fig. 8. All measurements are contained in the uncertainty of the dispersion measurement. The numerical artifacts do not significantly affect recorded dimensions and the method is considered robust in regard to projections during welding.
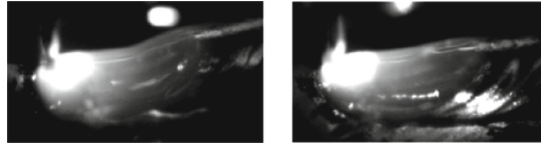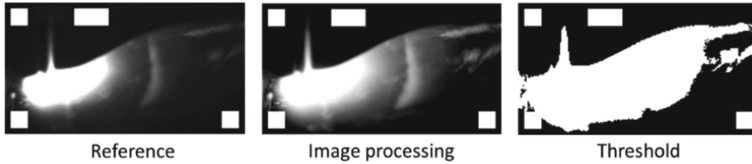
Fig. 6. Projection in valid images

Reference   Image processing   Threshold

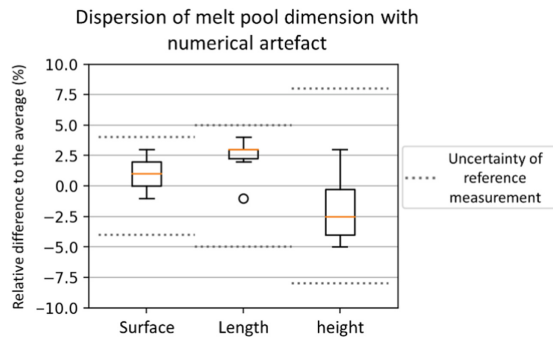**Fig. 7.** Numerical artifacts and numerical process

Fig. 8. Results for numerical artifacts

Size Variations of the Region of Interest

Because there is no physical trigger, maximizing the number of images between two arcs is important to obtain enough valid pictures. To do so, maximize the frame rate is a solution. The device has a maximal bandwidth which is defined as a function of the picture weight and the frame rate. As a consequence, choosing the right resolution can increase the frame rate. For each experiment, the resolution is optimized by enabling pixels in the ROI with the software of the camera. The influence of the size variations of the roi needs to be quantified. pictures of reference are modified by adding black pixels to the ROI until factors of 2 and 12 in size are reached. Pictures are gathered in Fig. 9 and results are presented in Fig. 10. According to the results, a size variation of the ROI does not significantly affect the dimensions. The method is then also considered robust against those deviations.

Reference   Size x2   Size x12

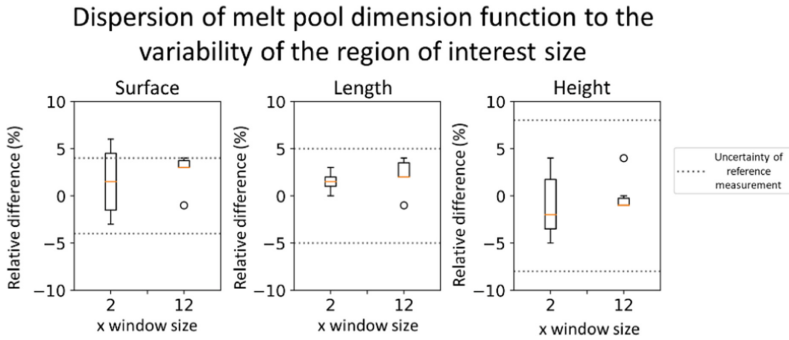**Fig. 9.** Numerical variability of the region of interest size

Fig. 10. Result for the numerical variability of the region of interest size

Blurry Pictures

If the melt pool is out of the focal plane, the picture is then blurry. To quantify this influence, a blur is generated numerically with a gaussian filter with the python library scipy.ndimage [17] using the function *guassian_filter* on pictures of reference. Three kinds of blurs are generated with different sigma (1, 3, 5) corresponding to a blur ever more important. Blurry pictures are gathered in Fig. 11 and results are shown in Fig. 12. The higher the blur is, the greater the dispersion on the surface is. Nevertheless, for a blur generated with a $\sigma = 1$, which is the most expected, no effect is detected. The method is considered robust as long as conditions are not too much deteriorated.
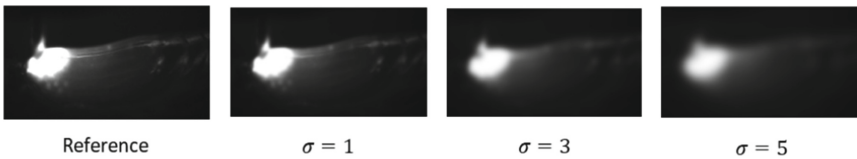

Reference $\sigma = 1$ $\sigma = 3$ $\sigma = 5$

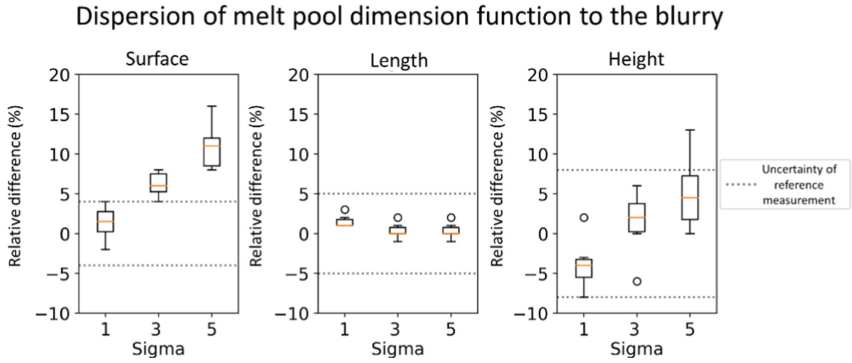**Fig. 11.** Numerical blurry function to sigma

Fig. 12. Result for numerical blurry

3.3 Sensitivity of the Method

To quantify the sensitivity of the method, three different cylinders are manufactured with different welding parameters. Three Wire Feed Speeds (WFS) are chosen: WFS equal to 6 m/min, 9 m/min and 12 m/min. The welding station worked in synergy mode. This means that the welding station automatically changes the energy function to WFS in order to weld correctly. The variation of the WFS significantly change the weld and it is used to quantify the sensibility of the device [18].

For this experiment, the number of active pixels on the camera changes to 360*214 pixels and the FPS to 550. The other processes and camera parameters stay unchanged. A picture of each experiment is given in Fig. 13 and the results are presented in Fig. 14. The result is manifest: the higher WFS is, the higher the dimensions of the thermal area are. We can clearly conclude that the method is sensitive to the WFS and therefore to melt pool variation.
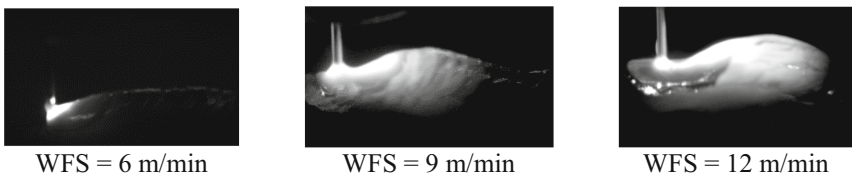

WFS = 6 m/min   WFS = 9 m/min   WFS = 12 m/min

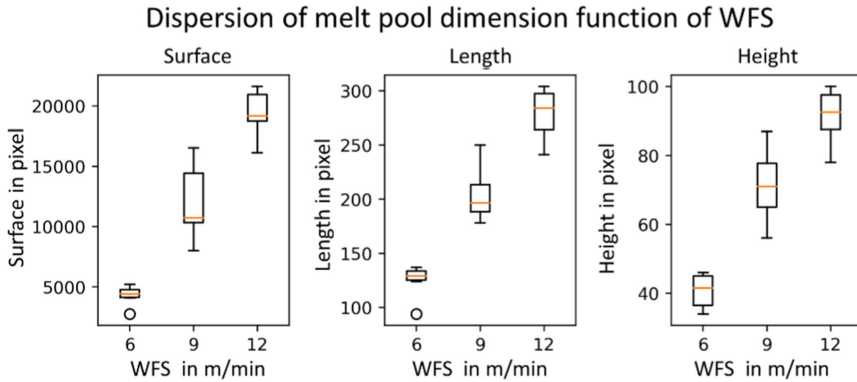**Fig. 13.** Size of the thermal area function to WFS

Fig. 14. Result for the size of the thermal area

4 Conclusion

A method has been presented in the paper to monitor aluminum melt pool during WAAM. An appropriate CMOS camera has been chosen to observe the near-infrared radiation of the melt pool using data from the literature and the expected physical characteristics of the observed melt pool. A numerical method has been developed to sort the images and then process them. Dimensional measurements characterize the thermal area. To evaluate the coherence between different measures, the repeatability was verified. Then the robustness has been evaluated on between three noticed noises: projections, size variation of the ROI and blur. Finally, the sensibility is validated studying the thermal dimension of melt pools caused by different WFS. Based on our experiment, we can conclude that measuring the melt pool with a CMOS camera is repeatable, robust and sensitive.

Furthermore, the study of the sensibility (Fig. 14) led us towards an interesting phenomenon. When the WFS is increased at 9 m/min and 12 m/min, our dimensional indicator dispersion increased which indicates melt pool instability. This is coherent with our knowledge of the process as we consider WFS = 6 m/min to be the optimal parameter. This observation is interesting and confirms the interest of this device for monitoring.

The feasibility of the melt pool acquisition using a near-infrared camera in aluminum Wire Arc Additive Manufacturing has been proved. An industrial prototype of the device can be developed by implementing a physical trigger realizing an automatic measurement of the thermal area dimensions and fixing it on the torch. It would be used for monitoring or closed loop control.

Finally, the same protocol can be performed for the steel alloy in order to compare the robustness and sensitivity of this device with the aluminum alloy.

References

1. Wu, B., et al.: A review of the wire arc additive manufacturing of metals: properties, defects and quality improvement. J. Manuf. Process. **35**, 127–139 (2018). https://doi.org/10.1016/j.jmapro.2018.08.001
2. Fronius: RCU 500i Operating instructions (2022). https://www.fronius.com/~/downloads/Perfect%20Welding/Operating%20Instructions/42,0426,0021,EN.pdf
3. Marinelli, G., Martina, F., Ganguly, S., Williams, S.: Development of wire + arc additive manufacturing for the production of large-scale unalloyed tungsten components. Int. J. Refract. Metals Hard Mater. **82**, 329–335 (2019). https://doi.org/10.1016/j.ijrmhm.2019.05.009
4. Béraud, N., Chergui, A., Limousin, M., Villeneuve, F., Vignat, F.: An indicator of porosity through simulation of melt pool volume in aluminum wire arc additive manufacturing. Mech. Ind. **23**, 1 (2022). https://doi.org/10.1051/meca/2021052
5. Ding, D., Pan, Z., Cuiuri, D., Li, H.: Wire-feed additive manufacturing of metal components: technologies, developments and future interests. The Int. J. Adv. Manuf. Technol. **81**(1–4), 465–481 (2015). https://doi.org/10.1007/s00170-015-7077-3
6. Chergui, M.A.: Simulation based deposition strategies evaluation and optimization in wire arc additive manufacturing (2021). https://tel.archives-ouvertes.fr/tel-03273221
7. Manokruang, S., Vignat, F., Museau, M., Limousin, M.: Process parameters effect on weld beads geometry deposited by wire and arc additive manufacturing (WAAM). In: Roucoules, L., Paredes, M., Eynard, B., Morer Camo, P., Rizzi, C. (eds.) JCM 2020. LNME, pp. 9–14. Springer, Cham (2021). https://doi.org/10.1007/978-3-030-70566-4_3
8. Everton, S.K., Hirsch, M., Stravroulakis, P., Leach, R.K., Clare, A.T.: Review of in-situ process monitoring and in-situ metrology for metal additive manufacturing. Mater. Des. **95**, 431–445 (2016). https://doi.org/10.1016/j.matdes.2016.01.099
9. Monier, R., Thumerel, F., Chapuis, J., Soulié, F., Bordreuil, C.: Liquid metals surface temperature fields measurements with a two-colour pyrometer. Measurement **101**, 72–80 (2017). https://doi.org/10.1016/j.measurement.2016.12.031
10. Halisch, C., Radel, T., Tyralla, D., Seefeld, T.: Measuring the melt pool size in a wire arc additive manufacturing process using a high dynamic range two-colored pyrometric camera. Weld. World **64**(8), 1349–1356 (2020). https://doi.org/10.1007/s40194-020-00892-5
11. Chen, M., Zhang, D., Wu, C.: Current waveform effects on CMT welding of mild steel. J. Mater. Process. Technol. **243**, 395–404 (2017). https://doi.org/10.1016/j.jmatprotec.2017.01.004
12. García, A., et al.: Online cracking detection by means of optical techniques in laser-cladding process. Struct. Control Health Monit. **26**(3), e2291 (2019). https://doi.org/10.1002/stc.2291
13. Xiong, J., Lei, Y., Chen, H., Zhang, G.: Fabrication of inclined thin-walled parts in multi-layer single-pass GMAW-based additive manufacturing with flat position deposition. J. Mater. Process. Technol. **240**, 397–403 (2017). https://doi.org/10.1016/j.jmatprotec.2016.10.019
14. Rouquette, S., Cambon, C., Bendaoud, I., Soulié, F.: Estimation of the heat source parameters during the deposition of SS316L wire with GMAW-CMT process: application to additive manufacturing; 28th Congress of French Thermal Society (2020). https://doi.org/10.25855/SFT2020-128
15. Schneider, C.A., Rasband, W.S., Eliceiri, K.W.: NIH Image to ImageJ: 25 years of image analysis. Nat Methods. **9**, 671–675 (2012). https://doi.org/10.1038/nmeth.2089
16. Frigge, M., Hoaglin, D.C., Iglewicz, B.: Some implementations of the boxplot. The Am. Stat. **43**(1), 50 (1989). https://doi.org/10.2307/2685173
17. Virtanen, P., et al.: SciPy 1.0: fundamental algorithms for scientific computing in Python. Nat. Methods **17**(3), 261–272 (2020). https://doi.org/10.1038/s41592-019-0686-2

18. Xia, C., Pan, Z., Zhang, S., Li, H., Xu, Y., Chen, S.: Model-free adaptive iterative learning control of melt pool width in wire arc additive manufacturing. The Int. J. Adv. Manuf. Technol. **110**(7–8), 2131–2142 (2020). https://doi.org/10.1007/s00170-020-05998-0